Iranian Journal of Materials Forming 13 (3) (2026) 34-51

Online ISSN: 2383-0042

IJMF

Iranian Journal of Materials Forming

Journal Homepage: http://ijmf.shirazu.ac.ir

Research Article

Development of the Maximum Rate of Dissipation Criterion to Analyze the Deformation Mechanisms in Semi-Solid State

Mohammad Hadi Sheikh Ansari and Mehrdad Aghaie Khafri*

Faculty of Materials Science and Engineering, K. N. Toosi University of Technology, Tehran 19991-43344, Iran

ARTICLE INFO

Article history:

Received: 30 November 2025
Reviewed: 9 February 2026
Revised: 26 February 2026
Accepted: 7 March 2026

Keywords:

Shear localization
Dilatancy
Dissipation
Internal friction
Semi-solid deformation

Please cite this article as:

Sheikh Ansari, M. H., & Aghaie Khafri, M. (2026). Development of the maximum rate of dissipation criterion to analyze the deformation mechanisms in semi-solid state. *Iranian Journal of Materials Forming*, *13*(3), 34-51. https://doi.org/10.22099/ijmf.2026.55062.1361

ABSTRACT

This study presents a new perspective on semi-solid rheology by applying the maximum dissipation rate criterion and stability analysis. Using this approach, we developed a criterion that identifies the conditions under which different deformation mechanisms dominate. A key finding is the critical role of rate-sensitivity in shaping both the mode and intensity of deformation. Specifically, we identify a threshold rate-sensitivity value of m = 0.21. Below this threshold, deformation is governed by granular processes such as grain rearrangement, jamming, and dilatancy. Above it, conversely, solid grains undergo plastic deformation instead. The analysis also establishes a strong correlation between dilatancy and rate-sensitivity. In the granular regime, higher rate dependency, resulting from increased solid fraction and stronger grain interconnections, promotes greater dilatancy and increased tendency for shear localization. At the critical threshold, localization emerges as bonds between grain agglomerates break, triggering Reynold's dilatancy. Collectively, these findings highlight that semi-solid materials exhibit granular-like behavior, wherein grain and agglomerate rearrangement, coupled with dilatancy, drive the transition toward shear banding following the failure of inter-particle bonds. These insights provide a clearer framework for understanding and predicting the complex behavior of semi-solid materials under load.

Nomenclature

f_L	Fraction of the liquid phase	F	Deformation gradient
f	Total fraction of porosities and liquid phase	D	Rate of deformation
f_s^{coh}	Shear coherency solid fraction	Υ	Norm of the rate of deformation
θ	Rate of dissipation	n	Normal of the rate of deformation
S	Stress tensor	$\dot{\varepsilon}$	Equivalent strain rate
E	Strain tensor	ψ	Fraction of the solid skeleton
ρ_0	Density	ψ_{cr}	Critical value of the fraction of the solid skeleton
H	Helmholtz free energy	β	Dilatancy value
g	Natural deformation gradient	α	Flow localization parameter
A	Driving force	α_{cr}	Critical value of the flow localization parameter
$A(f_s)$	A function of the solid fraction, $A(f_s)=\frac{3}{f_s^5}$ in Nguyen model	m	Strain rate sensitivity parameter
L	Velocity gradient	η	Efficiency of the power dissipation

* Corresponding author
E-mail address: maghaei@kntu.ac.ir (M. Aghaie Khafri)
https://doi.org/10.22099/ijmf.2026.55062.1361

1. Introduction

The deformation of alloys in the semi-solid state exhibits pseudoplastic behavior, leading to more controllable die filling compared to conventional casting processes. Furthermore, it enables the production of complex-shaped components using significantly lower forces than common solid-state forming processes, such as forging. This particular rheological property stems from the thixotropic nature of alloys with a granular microstructure in the semi-solid state [1-6]. At rest, the grains connect to form a continuous, load-bearing solid skeleton of interconnected grains or agglomerates. The general consensus has been that the shear thinning property originates from the breakdown of the bonds between these agglomerates under shear. Based on this concept, numerous thixotropic models have been successfully developed to capture the complex rheology under both steady-state and transient conditions [7-12].

However, as revealed by Gourlay et al. [13] in their pioneering work, the deformation of alloys in the semi-solid state, above the shear coherency fraction, f_s^{coh}, is associated with granular features such as shear induced dilation and jamming. The coherency fraction is the critical solid fraction above which individual grains or crystals coalesce to form a load-bearing, interconnected solid skeleton. For a granular microstructure (typical for semi-solid deformation), this value is approximately 0.4. Using synchrotron X-ray tomography, Kareh et al. [14] demonstrated that the compression forces applied to alloys in the semi-solid state can open internal pores via Reynold's dilatancy. This is a phenomenon observed in granular materials where the material tends to increase in volume (dilate) when subjected to shear deformation, whereby the solid density moves towards a critical value analogous to that of soils. Subsequently, Su et al. [15] studied the rheological transitions of semi-solid deformation from low to high solid fractions by using the synchrotron tomography combined with Lattice Boltzmann Method - Discrete Element Method (LBM-DEM) simulation. They revealed that the onset of shear localization is associated with time-dependent processes of local dilatancy and a drop in liquid pressure. In a similar work, Su et al. [16] demonstrated via DEM simulation that the deformation behavior of semi-solid alloys can be analyzed within the framework of critical state soil mechanics.

On the other hand, the occurrence of shear localization is associated with a sudden drop in stress after reaching a peak at very low strains. This behavior is attributed to the breakdown of the solid skeleton formed prior to the onset of deformation. As mentioned, this softening phenomenon is a consequence of two mechanisms: (a) decohesion, represented by a rate-type equation in thixotropic models, or (b) the rearrangement of grains and agglomerates, accompanied by dilatancy and subsequent shear banding, as observed in saturated granular materials. The authors have developed shear localization criteria based on each of these two assumptions, employing analytical approaches such as linear perturbation analysis, bifurcation theory, and the thermodynamic concept of maximum dissipation rate [17-20]. However, the correlation between these two proposed softening mechanisms remains unclear. Moreover, at high solid fraction, semi-solid deformation can lead to plastic deformation within the solid grains themselves. Plastic deformation in semi-solid alloys is significantly influenced by grain boundaries, which serve sources of dislocations. This is particularly evident under severe plastic deformation, where the "interfacial fluid" concept enables continuous solid-state flow capable of accommodating large strains [21]. Although both granular behavior and plastic deformation of grains have been extensively studied, no suitable analytical criterion has yet been developed to determine the conditions under which each mechanism dominates. In the present study, by employing a rheological constitutive model and applying the thermodynamic concept of maximum dissipation rate, a new interpretation of deformation mechanisms in the semi-solid state is proposed, addressing the occurrence of shear localization and the role of softening mechanisms. Experimental studies, such as those by Gourlay et al. [13], Kareh et al. [14], and Su et al. [15, 16], have established that deformation behavior in the semi-solid state is strongly governed by the arrangement, morphology, and interaction of solid grains and

agglomerates. These factors directly affect phenomena like dilatancy, jamming, and shear localization. In this study, a continuum-based modeling approach is employed, in which microstructural effects are incorporated implicitly through averaged material parameters. Consequently, whereas the established connections offer significant insight into macroscopic rheological behavior and the initiation of localization, they fail to directly represent localized, microstructurally driven mechanisms inherent to heterogeneous grain structures. The discussion presents a comprehensive comparison between the model's projected trends and the results of in-situ experimental investigations. Future advancements may integrate explicit microstructural descriptors, potentially through discrete element or micromechanical modeling frameworks, to address this gap and improve predictive capability for systems in which grain arrangement play a critical role.

2. Maximum Rate of Dissipation Criterion

Ziegler [22, 23] argued that, according to the orthogonality condition in an extremum continuum framework, flow stability requires the internal entropy production rate to equal or exceed the applied entropy rate. Otherwise, instability occurs. In other words, for a stable flow, the actual velocity (or strain rate) within a velocity field maximizes the dissipation rate. This statement outlines the principle of the maximum rate of dissipation. Notably, Ziegler derived the dissipation rate principle as a necessary consequence of the assumed orthogonality condition. In contrast, Rajagopal and Srinivasa [24, 25] treated the maximum dissipation rate as a thermodynamic concept, developing a finite deformation framework to show that normality and convexity are necessary and sufficient conditions for this principle. They stated that the rate of dissipation can be expressed as the difference between the mechanical power and the rate of variation of Helmholtz potential:

$$\Theta = S:\dot{E} - \rho_0\dot{H} \geq 0 \tag{1}$$

Where Θ, S, E, ρ_0, and H denote the rate of dissipation, stress tensor, strain tensor, density, and Helmholtz free energy, respectively. Helmholtz potential is a part of internal energy that measures the work at constant temperature. The change in the Helmholtz energy during a process is equal to the maximum amount of work that the system can perform in a thermodynamic process in which temperature is held constant. This function depends on the current state of a system, indicated by strain tensor (E). It also depends on another internal variable (g), the natural deformation gradient, which represents the gradient of mapping from the initial configuration to the current natural configuration. Thus:

$$H = H(E, g) \tag{2}$$

In the framework of classical plasticity, the tensor g identifies the plastic deformation, i.e. the plastic strain. The evolution of the natural configuration (the rate of change of g) expressed via the plastic velocity gradient, which depends on the current configuration as well as the deformation gradient from it:

$$L_p = L_p(E, g) \tag{3}$$

While stored energy applies to both deformation modes, the presence of dissipation is what specifically characterizes and separates inelastic deformation from elastic behavior. Therefore, the rate of dissipation is independent of the current state of the system (E) and only depends on the plastic deformation gradient (g) and also the plastic velocity gradient (L_p), associated with the microstructural variations. According to the dependency of H on E and g, Eq. (1) can be rewritten as below:

$$S:\dot{E} - \rho_0\left(\frac{\partial H}{\partial E}:\dot{E} + \frac{\partial H}{\partial g}\dot{g}\right) = \Theta(g, L_p) \tag{4}$$

The above equation should be satisfied for all values of $\dot{E}$. This implies that:

$$S = \rho_0\frac{\partial H}{\partial E} \tag{5}$$

By introducing the driving force, A, as $A(E, g) = -\rho_0\frac{\partial H}{\partial g}g^T$ and considering the relation of $L_p = \dot{g}g^{-1}$, the below relation for the rate of dissipation is finally obtained:

$$\Theta\left(g, L_p\right) = A(E, g): L_p \tag{6}$$

Let $L_p = L_p(E, g)$ be the actual value of plastic part of velocity gradient. The principle of maximum rate of dissipation implies that if L_1 is any other velocity gradient with greater rate of dissipation than actual one, then:

$$A(E, g): L_1 < \Theta(g, L_1) \tag{7}$$

In other words, if Υ is introduced as the norm of the rate of deformation ($\Upsilon = \|D_p\| > 0$), where D_p is the symmetric part of L_p, increasing Υ leads that the rate of dissipation increases faster than the energy release rate. This statement can be expressed mathematically as:

$$\frac{\partial \Theta}{\partial \Upsilon} > \frac{\partial (A: D_p)}{\partial \Upsilon} \tag{8}$$

In above equation, A is independent of D_p and so Υ. Thus, Eq. (8) is reduced to:

$$\frac{\partial \Theta}{\partial \Upsilon} > A: \frac{\partial D_p}{\partial \Upsilon} \tag{9}$$

According to Eq. (6) and introducing the normal of the rate of deformation, $n = \frac{D_p}{\|D_p\|} = \frac{D_p}{\Upsilon}$, Eq. (9) can be rewritten as:

$$\frac{\partial \Theta}{\partial \Upsilon} > A: n \tag{10}$$

Consequently, the stability condition can be derived by considering the relation between n and D_p:

$$\frac{\partial \Theta}{\partial \Upsilon} > \frac{\Theta}{\Upsilon} \tag{11}$$

A fundamental requirement in plasticity is that the driving force must be work-conjugate to the plastic strain. By taking the rate of deformation, D, as the plastic strain measure, the Cauchy stress, σ, can be considered as its conjugate pair. Introducing the strain rate equivalent as $\dot{\varepsilon} = \sqrt{(2/3)}\,\|D\|$ and neglecting the elastic part, the onset of localization can be briefly expressed as:

$$\frac{\partial \Theta}{\partial \dot{\varepsilon}} = \frac{\Theta}{\dot{\varepsilon}} \tag{12}$$

It is noteworthy that in the relation of the von Mises equivalent strain rate, $\dot{\varepsilon} = \sqrt{(2/3)}\,\|D\|$, $\|D\| = \sqrt{D: D}$, denotes its Euclidean norm. This definition follows directly from J_2 plasticity theory and ensures that for uniaxial compression, $\dot{\varepsilon}$ equals the axial strain rate. The factor 2/3 arises from the relationship between the norm of the deviatoric strain rate tensor and the axial strain rate under incompressible, axisymmetric deformation. This scalar measure of deformation intensity is work-conjugate to the von Mises equivalent stress, guaranteeing that the plastic work rate is correctly represented as $\dot{W}^p = \bar{\sigma}\dot{\bar{\varepsilon}}$.

3. Constitutive Equation for Semi-Solid Deformation

Under uniaxial compressive loading, the deformation of semi-solid materials is assumed to occur very low segregation as revealed by Suery and Flemings [26]. By considering the fact that the instability of a semi-solid material under these conditions occurs at very low strains, the undrained condition is assumed for the deformation at least up to the strain levels where localization may occur. The strain rate is also an important parameter. In this study, the undrained assumption is considered valid for strain rates of approximately 10^{-2} s^{-1} and higher. This lower bound is based on the work of Suery and Flemings [26], who showed that above this threshold, liquid segregation becomes negligible and deformation remains homogeneous. Experimental studies reporting granular-type deformation under undrained conditions [14, 27] were conducted within this regime, confirming its practical relevance. Although the present analysis focuses on undrained conditions, it is important to acknowledge that liquid segregation can become significant at lower strain rates or during prolonged deformation. When segregation occurs, the liquid phase is squeezed out of the deforming region, leading to a local increase in solid fraction.

Before presenting the constitutive model, it is important to clarify the strain rate notation used throughout this work. Two related measures of deformation rate are:

- $\dot{\varepsilon}$: The von Mises equivalent strain rate, defined in section 2 as $\dot{\varepsilon} = \sqrt{(2/3)}\,\|D\|$. This quantity equals the axial strain rate in uniaxial compression and is

work-conjugate to the von Mises equivalent stress.

- $\dot{\gamma}$: The equivalent shear strain rate, commonly used in the Nguyen constitutive model [27]. The two measures are related by $\dot{\gamma} = \sqrt{3}\dot{\varepsilon}$, which ensures that the dissipation rate is invariant $\Theta = \tau\dot{\gamma} = \sigma\dot{\varepsilon}$, where τ is the shear stress and σ is the equivalent tensile stress.

In the following derivations, $\dot{\gamma}$ is used when working directly with the Nguyen model, while $\dot{\varepsilon}$ appears in the general dissipation criterion. The relationship between them is applied consistently to maintain physical consistency throughout the analysis.

In the present study, a model developed by Nguyen et al. [28] has been considered. This model was proposed for the deformation of semi-solid alloys at high solid fraction using the mixture theory in which two phases of solid and liquid are considered as contiguous. The Nguyen model incorporates key features that are essential for analyzing deformation mechanisms at high solid fractions:

- Viscoplastic flow behavior with rate-sensitive response, which is critical for understanding the role of strain rate-sensitivity in the granular-to-plastic transition.
- Solid fraction dependence through the function $A(f_s)$, which captures the strengthening effect of the solid skeleton.
- Thermodynamic consistency, allowing integration with the maximum dissipation rate criterion.
- Experimental validation across multiple alloy systems (Sn-Pb, Al-Cu) in the high solid fraction regime [28, 29].

Under undrained deformation, the constitutive equation based on the associated flow rule can be written as:

$$\dot{\gamma} = [\alpha'^{n'} C\, exp(\frac{-Q}{RT})(\frac{A(f_s)}{3})^{\frac{n+1}{2}}]\tau^{n'} \quad (13)$$

Where $\dot{\gamma}$ is the equivalent shear strain rate (s^{-1}), τ is the equivalent shear stress (MPa), α' is a material constant related to the reference strain rate (dimensionless), n' is the stress exponent, related to the strain rate sensitivity parameter m via $m = 1/n'$, C is a material constant, Q is the activation energy for deformation (J/mol or kJ/mol), R = 8.314 J/mol.K is the universal gas constant, T is the absolute temperature (K), n is an exponent in the solid fraction function (not to be confused with n'), $A(f_s)$ is a function of the solid fraction f_s, defined below in Eq. (14):

$$A(f_s) = \frac{3}{f_s^{\varsigma}} \quad (14)$$

Where ς is taken to be 8.5, based on the experiments performed by Martin et al. [28]. Eq. (13) can be rewritten as:

$$\tau = \frac{1}{\alpha'}[\frac{1}{C} exp(\frac{Q}{RT})]^m f_s^{\frac{\varsigma(1+m)}{2}} \dot{\gamma}^m \quad (15)$$

It is important to note that the present analysis is specifically concerned with semi-solid deformation at high solid fractions, where the transition between granular flow and grain plasticity occurs. This regime corresponds precisely to the conditions for which the Nguyen model was originally developed and validated. As demonstrated by Gourlay et al. [13], Kareh et al. [14], and Su et al. [15, 16], the granular deformation mechanisms, including dilatancy, jamming, and shear localization, are most prominent at solid fractions above the shear coherency point ($f_s > 0.4$) and become dominant at $f_s > 0.6$. Therefore, the Nguyen model is not being applied outside its intended scope; rather, it is being used precisely within the regime for which it was designed. For applications outside this regime, particularly at lower solid fractions or under partially drained conditions, the model should be extended.

A key advantage of the Nguyen model for our purpose is that it yields a closed-form expression for the dissipation function (Eq. (16)), which is essential for applying the maximum dissipation rate criterion (Eq. (12)). This analytical tractability allows us to derive explicit conditions for shear localization and the critical rate-sensitivity threshold without resorting to numerical simulations, thereby, providing clear physical insights into the underlying mechanisms. As stated in previous section, the dissipation function can be determined by having the conjugate pair of the deformation gradient, or

the strain rate equivalent, and the Cauchy stress. Therefore, in the aforementioned one-dimensional problem, the dissipation function can be obtained as the product of conjugate pair of $\dot{\gamma}$ and τ. By substituting Eq. (15) into the dissipation function formulation, the product of stress and equivalent strain rate directly expresses the rate of dissipation as a function of strain rate and rate-sensitivity parameter, as follows:

$$\Theta = \tau\dot{\gamma} = \frac{1}{\acute{\alpha}}[\frac{1}{C}exp(\frac{Q}{RT})]^m f_s^{\frac{\varsigma(1+m)}{2}}\dot{\gamma}^{m+1} \quad (16)$$

Since the constitutive relation from Nguyen et al. [28] defines stress explicitly as a function of strain rate and solid fraction, it enables a closed-form dissipation function that can be used within the maximum dissipation criterion (Eq. (12)) to derive the localization condition.

4. Shear Localization Analysis

The onset of shear localization as a type of flow instability can be expressed by Eq. (12). Substituting Eq. (15) into Eq. (16) and applying the localization condition from Eq. (12), the onset of localization can be assessed in terms of the known parameters of the constitutive model, namely the rate-sensitivity m and solid fraction f_s:

$$\frac{\partial\Theta}{\partial\dot{\gamma}} = \frac{m+1}{\acute{\alpha}}\left[\frac{1}{C}\exp\left(\frac{Q}{RT}\right)\right]^m f_s^{\frac{\varsigma(1+m)}{2}}\dot{\gamma}^m + \frac{\varsigma(1+m)}{2\acute{\alpha}}\left[\frac{1}{C}\exp\left(\frac{Q}{RT}\right)\right]^m f_s^{\frac{\varsigma(1+m)}{2}}\dot{\gamma}^{m+1}\frac{df_s}{d\dot{\gamma}} = \frac{\Theta}{\dot{\gamma}} = \frac{1}{\acute{\alpha}}[\frac{1}{C}\exp\left(\frac{Q}{RT}\right)]^m f_s^{\frac{\varsigma(1+m)}{2}}\dot{\gamma}^m \quad (17)$$

Results in:

$$mf_s + \frac{\varsigma}{2}(1+m)\dot{\gamma}\frac{df_s}{d\dot{\gamma}} = 0 \quad (18)$$

By considering $f_s = 1 - f_L$, Eq. (17) reduces to:

$$m(1-f_L) - \frac{\varsigma}{2}(1+m)\dot{\gamma}\frac{df_L}{d\dot{\gamma}} = 0 \quad (19)$$

Eq. (19) essentially gives a quantitative criterion to assess whether the current state of the material (defined by m and f_L) has reached the localization threshold. The localization appears as a dilatant shear band, in which the fraction of porosities is locally increased. The model variable f describes the total fraction of porosity and liquid, with an initial value f_L. Hence, Eq. (19) can be rewritten as:

$$m(1-f) - \frac{\varsigma}{2}(1+m)\dot{\gamma}\frac{df}{d\dot{\gamma}} = 0 \quad (20)$$

Similar to porous materials, (e.g., [29]) in which the dilatational strain rate controls the rate of void volume change in the matrix ($\dot{f} = (1-f)tr(\dot{\varepsilon})$), the variation of f can be expressed by a differential equation:

$$\dot{f} = (1-f)\psi\beta\dot{\gamma} \quad (21)$$

Where β represents the dilatancy value, obtained as a ratio of the hydrostatic strain (rate) to the deviatoric one. Therefore, $\beta\dot{\gamma}$ indicates the normal strain rate. In addition, ψ refers to the fraction of the solid skeleton, consisting of agglomerates interconnected by cohesive bonds. In other words, ψ represents the volume fraction of solid grains that form a continuous, load-bearing network. This concept distinguishes between:

- Isolated grains: Solid particles that are surrounded by liquid and do not contribute to stress transmission.
- Interconnected grains: Solid particles that are in direct contact with neighbors, forming a percolating network capable of supporting mechanical loads.

This parameter represents the dependency of local dilatancy to the fraction of the solid skeleton, in such a way that dilatancy disappears when $\psi \to 0$. The initial value of ψ depends on the solid fraction and is expressed as:

$$\psi_{init} = 1 - \frac{f_s^{coh}}{f_s} \quad (22)$$

Where f_s^{coh} is the shear coherency fraction (≈ 0.4 for granular microstructures [13]). Equation (22) provides a phenomenological mapping between the total solid fraction f_s and the fraction of the solid skeleton, ψ_{init}, accounting for the fact that not all solid particles participate in the connected network at lower f_s. On the other hand, according to synchrotron tomography

observations by Kareh et al. [14], a continuous force-carrying skeleton forms at a critical solid fraction $f_s \approx 0.62$, above which dilatant shear bands and localization appear. Therefore, by taking f_s^{crit} in Eq. (22), ψ_{cr} becomes 0.35. This value therefore represents the critical percolation level of the solid skeleton and is not an adjustable parameter. Since f is a function of both strain rate $\dot{\gamma}$ and strain γ, the total derivative $df/d\dot{\gamma}$ accounts for both explicit and implicit dependencies. Using the chain rule, the complete differential of $df/d\dot{\gamma}$ (in Eq. (20)) can be represented by the following equation:

$$\frac{df}{d\dot{\gamma}} = \frac{\partial f}{\partial \dot{\gamma}} + \frac{\partial f}{\partial \gamma}\frac{d\gamma}{d\dot{\gamma}} \tag{23}$$

The fraction of porosity, f is not implicitly formulated in terms of $\dot{\gamma}$; so $\frac{\partial f}{\partial \dot{\gamma}} = 0$. By applying the partial time derivative to both numerator and denominator of $\frac{\partial f}{\partial \gamma}$, i.e. $\frac{\partial \dot{f}}{\partial \dot{\gamma}}$ and using Eq. (21):

$$\frac{df}{d\dot{\gamma}} = (1-f)\psi\beta\frac{\mathrm{d}\gamma}{\mathrm{d}\dot{\gamma}} \tag{24}$$

Accordingly, Eq. (20) can be reformulated as:

$$m - \frac{\varsigma}{2}(1+m)\psi\beta\dot{\gamma}\frac{d\gamma}{d\dot{\gamma}} = 0 \tag{25}$$

To simplify further and characterize the relative rate of porosity generation to strain, we introduce the localization parameter, α, as $\alpha = \frac{1}{\dot{\gamma}}\frac{d\dot{\gamma}}{d\gamma}$, Eq. (25) becomes:

$$\alpha = \frac{\varsigma}{2}\frac{(1+m)}{m}\psi\beta \tag{26}$$

The localization parameter is a dimensionless scalar quantity used to characterize the material's susceptibility to a strain localization, typically in the form of shear bands. In other words, it quantifies the intensity of strain rate concentration during deformation. It measures how rapidly the strain rate increases as deformation progresses. When α is small, the strain rate remains relatively constant, indicating homogeneous deformation. Otherwise, at high values of α, the strain rate accelerates rapidly with increasing strain, indicating the onset of strain localization into a narrow band. This parameter is analogous to the strain rate sensitivity index used in classical formability analysis, where the tendency for necking in tensile deformation is related to the rate at which strain concentrates. In both cases, a higher value indicates greater susceptibility to localization. It should be noted that while the derivative $d\dot{\gamma}/d\gamma$ does not represent a direct physical quantity in the classical sense, it is introduced here as part of the localization parameter formulation, analogous to its role in classical formability analysis and flow instability criteria, where such terms quantify the sensitivity of strain accumulation to changes in strain rate at the onset of localization. In our previous article [17], we showed that the shear localization occurs at $\alpha > 5$, so the critical value, i.e. the minimum value, for the shear localization is taken to be 5 ($\alpha = 5$), i.e.:

$$\alpha_{cr} = \frac{\varsigma}{2}\frac{(1+m)}{m}\psi\beta = 5 \tag{27}$$

This critical value is consistent with the critical value of the fraction of the solid skeleton, ψ_{cr} (≈ 0.35). Finally, by rearranging Eq. (27) for the dilatancy value and inserting the critical values of α_{cr} and ψ_{cr}, the result is:

$$\beta = \frac{2m\alpha_{cr}}{\varsigma(1+m)\psi_{cr}} \tag{28}$$

Taking ς, α_{cr}, and ψ_{cr} as 8.5, 5, and 0.35, the dilatancy value is obtained as a function of the rate sensitivity:

$$\beta = 3.36\frac{m}{1+m} \tag{29}$$

On the other hand, under undrained condition, the associated flow rule implies that $\beta = \mu$ [30], where μ is the internal friction. The deformation behavior of solid grains and inter-particle bonds in cohesive granular systems can be effectively described using the Hosford yield criterion [31], which generalizes the von Mises formulation by introducing an exponent *n* that controls the shape of the yield surface in principal stress space. The criterion is expressed as:

$$[((\sigma_1-\sigma_2)^n + (\sigma_1-\sigma_3)^n + (\sigma_2-\sigma_3)^n)/2]^{1/n} = Y \tag{30}$$

Where $\sigma_1, \sigma_2, \sigma_3$ are the principal stresses and Y is the uniaxial yield stress. As established by Butcher and

Abedini [32], the exponent n dictates the ratio of shear stress to uniaxial yield stress, effectively linking the yield surface shape to the material's internal cohesive friction coefficient, μ. In the quadratic form (n = 2), the Hosford criterion reduces to the classical von Mises model with $\mu = 0.58$. However, for body-centered cubic (BCC) and face-centered cubic (FCC) metals, higher values of n have been recommended to better capture their yielding characteristics, with corresponding reductions in internal cohesive friction. Specifically, values of n = 6 and n = 8 have been suggested for BCC and FCC metals, yielding $\mu = 0.56$ and $\mu = 0.545$, respectively. Based on the fact that β has a maximum value of 0.58, (from the von Mises criterion), it is possible to consider an upper bound for the rate sensitivity of semi-solid granular deformation ($m \approx 0.21$). Eq. (29) presents an interesting result because it establishes a relation between the rate-sensitivity of alloys before the softening state, commonly measured at the peak stress, and the dilatancy at the softening stage. This equation indicates that at high solid fraction, where the rate-sensitivity has higher values (see, for example, the experimental study of Freitas and Ferante [33]), more dilatancy and consequently a stronger tendency for shear localization are expected. This result is in consistent with X-ray tomography experiments [14, 34, 35], which demonstrate that localization and crack formation intensify with increasing solid fraction. In another work, Wu et al. [36] investigated the deformation behavior of sintered porous 2024 aluminum alloy in the semi-solid state. The study revealed that deformation at high solid fractions exhibits rate sensitivities below 0.15, and as predicted by the present criterion, the thixotropic softening behavior is observed as the dominant feature of granular deformation. Eq. (29) also reveals that cohesion between the solid grains and agglomerates intensifies the occurrence of shear localization. In this case, the rearrangement of agglomerates and further dilatancy requires overcoming internal friction between particles and breaking the cohesive bonds. Our previous analytical studies [19, 20], yielded similar conclusions.

Beyond this limit (m > 0.21), the stress state increasingly approaches a pure deviatoric form, characteristic of the plastic deformation of solid grains, rather than granular rearrangement mechanisms. This transition is consistent with the experimental findings of Tzimas and Zavaliangos [27], who conducted compression tests on A2014 and Al-4 wt.% Cu alloys in both fully solid and semi-solid states at high solid fractions. Their results indicated that the instantaneous strain rate sensitivity parameter (m) remained approximately 0.22 in the semi-solid state at high solid fractions (fs > 0.8) and approached 0.25-0.3 in the fully solid state at 500 °C. While their study did not explicitly report a critical m value demarcating the transition between granular and plastic deformation, their observations of increased localization and damage at high solid fractions, along with a shift to ductile behavior at lower f_s, indirectly support the idea of a deformation mode transition governed by rate sensitivity. This correlation reinforces the present study's proposition that a critical m value of approximately 0.21 could serve as a practical indicator for the onset of plastic deformation dominance in semi-solid alloys. Furthermore, the qualitative trends in localization, damage, and dilatancy behavior reported by Tzimas and Zavaliangos [27] agree with the predicted evolution of deformation mechanisms proposed in the present analysis. Additional comparison with the experimental results of Zhang et al. [37] strengthens the validity of the proposed critical strain rate sensitivity parameter ($m \approx 0.21$) as a threshold for deformation mechanism transitions in semi-solid alloys. Their thorough investigation of A356.2 alloy under high solid fraction compression found an unambiguous relationship between compression velocity, deformation zone characteristics, and the strain rate sensitivity parameter. Consistent with the predominantly solid-like behavior reported by Tzimas and Zavaliangos [27] and projected by the present analysis for m > 0.21, their results revealed an average m value of approximately 0.2757 under conditions favoring plastic deformation of solid grains within severe deformation zones. Other experimental studies [38-41] revealed that the plastic deformation of alloys in the semi-solid state is associated with dislocation pile-up and the occurrence of dynamic

restoration mechanisms. Table 1 summarizes these datasets, spanning multiple alloy systems, solid fractions, and experimental conditions.

Based on the above analysis, it can be stated that the types of deformation mechanisms, granular or plastic mechanisms, and their intensities can be evaluated solely from the rate-sensitivity, which may change during deformation (the evaluation should therefor be performed for a specific strain, e.g. the strain corresponding to the peak stress). The overall trend of the deformation mechanisms is summarized in Fig. 1.

The transition between these regimes is modulated by microstructural parameters, particularly particle size. Finer microstructures, such as AA2024 with an average particle size of 49 μm, increase m to values around 0.26 by reinforcing the solid skeleton, while coarser structures (e.g., Al-4% Cu at 84 μm) reduce m to 0.14-0.17, promoting granular flow characteristics [33]. This interplay of deformation mechanisms, quantified through strain rate jump tests and microstructure-sensitive constitutive modeling [28] supports $m \approx 0.21$ as a reliable indicator of shifts in dissipation pathways in semi-solid alloys.

It is important to note that while Eq. (29) is derived within the framework of the Nguyen et al. constitutive model, its qualitative implications, such as the correlation between dilatancy and rate-sensitivity and the existence of a critical rate-sensitivity value, are consistent with broader granular mechanics principles, particularly those described in critical state soil mechanics. Future studies should investigate whether this relationship holds for other semi-solid constitutive models based on similar assumptions.

Solving Eq. (29) for the rate-sensitivity exponent m yields the following expression for the critical value m_c:

$$m_c = \frac{1}{\frac{2\alpha_{cr}}{\beta_{max}\varsigma\psi_{cr}} - 1} \tag{31}$$

To assess the robustness of the predicted critical rate-sensitivity threshold ($m_c \approx 0.21$), a One-At-a-Time (OAT) sensitivity analysis was performed on the four key parameters that influence Eq. (29); the solid fraction exponent ς, the critical localization parameter α_{cr}, the critical solid skeleton fraction ψ_{cr}, and the maximum dilatancy β_{max} derived from the yield criterion. Each parameter was varied independently over a range consistent with experimental and theoretical studies in the literature (Table 2). The resulting m_c values remained within 0.16-0.27, with a central tendency of 0.21-0.22. This narrow variation confirms that the proposed threshold is not an artifact of specific parameter choices but a stable feature of the dissipation-based criterion. The analysis further indicates that m_c is most sensitive to the localization intensity, α_{cr} and the solid fraction hardening parameter, ς, reflecting the dominant role of strain localization intensity and solid skeleton hardening in the granular-to-plastic transition. A steeper solid fraction dependence makes the skeleton stronger, delaying the switch to plasticity. The critical solid skeleton fraction ψ_{cr} also exerts a substantial influence on m_c, with only a modest difference compared with the

Table 1. Experimental studies reporting rate-sensitivity values and corresponding deformation mechanism

Alloy system	Solid fraction (f_s)	Reported m value	Observed deformation mechanism	Reference
Sintered porous 2024 Al alloy	High	< 0.15	Granular (thixotropic softening)	Wu et al. [36]
Al-4% Cu (coarse grains, 84 μm)	0.65-0.85	0.14-0.17	Granular flow	Ferrante & De Freitas [33]
Al-4% Cu (fine grains, 49 μm)	0.65-0.85	~ 0.26	Mixed/ transitional	Ferrante & De Freitas [33]
Al-4% Cu, A2014	> 0.8	~ 0.22	Transitional (both granular and plastic features)	Tzimas & Zavaliangos [37]
A356.2	High	0.2757 (Average)	Plastic deformation dominant	Zhang et al. [38]

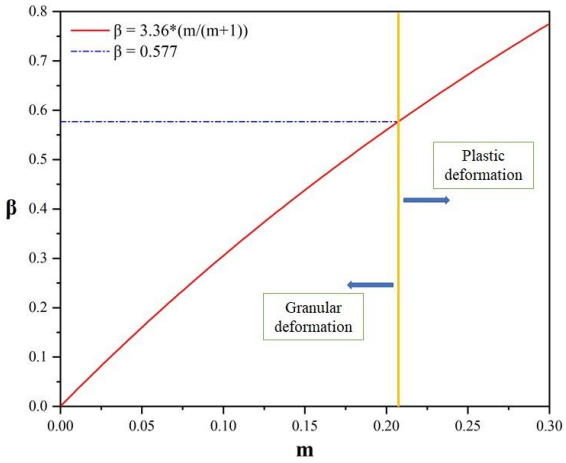

Fig. 1. Variation of the dilatancy value versus the rate-sensitivity.

Table 2. Sensitivity of the critical rate-sensitivity m_c to key model parameters

Parameter	Range tested	Corresponding m_c range
ς	7-10	0.16-0.25
α_{cr}	4-6	0.17-0.27
ψ_{cr}	0.3-0.4	0.17-0.24
β_{max}	0.545-0.58 (Depending on yield surface shape)	0.19-0.21

previous parameters. This indicates that the percolation threshold, the solid fraction at which a continuous, load-bearing network forms, is not merely a boundary condition but an active contributor to the transition mechanism. A higher ψ_{cr} delays the onset of dilatancy and shear banding, thereby shifting the critical rate-sensitivity toward higher values. In contrast, the maximum dilatancy β_{max} shows comparatively weaker sensitivity, suggesting that while it defines the ultimate limit of the granular regime, the precise location of the m_c threshold is more strongly governed by the evolution of localization and skeleton connectivity prior to reaching that limit.

It is noteworthy to mention that this finding, namely, the critical role of the rate-sensitivity in predicting the deformation mechanisms in semi-solid state, is analogous to the results obtained using the approach of dynamic materials modeling (DMM), proposed for the prediction of microstructural changes during hot working. Based on DMM approach, viscoplastic deformation dissipates power through heat conduction and microstructural evolution. The efficiency of deformation is defined as a function of rate-sensitivity. This efficiency parameter serves as a key indicator for identifying dominant deformation mechanisms [42-47]. Although the approach followed in this paper is different from that of the maximum rate of dissipation criterion, and deformation is more complex in the semi-solid state, both approaches establish frameworks for predicting deformation mechanisms based on rate-sensitivity.

The dissipation-based criterion developed in this study combines two essential components: (i) the thermodynamic maximum dissipation principle, and (ii) a specific constitutive model (Nguyen et al. [28]) describing the rheological behavior of semi-solid alloys. To assess the generalizability of the approach, it is useful to distinguish between these components and examine which elements are model-dependent and which are transferable to other constitutive descriptions. The maximum dissipation principle is a fundamental thermodynamic postulate that does not depend on a specific constitutive model. It states that for a given thermodynamic state, the actual dissipation rate maximizes the dissipation potential among all admissible kinetic processes. Therefore, the core methodology, equating the marginal dissipation rate to the average dissipation rate, can be applied to any constitutive model that provides a closed-form or computationally tractable expression for the dissipation function. This thermodynamic foundation ensures that the approach is not limited to the Nguyen model but has broad applicability across material classes. To apply the proposed criterion to a different constitutive model, the following conditions (Table 3) must be satisfied.

5. Summary of Equation Origins and Novel Contributions

To provide full transparency and clearly distinguish between established results from the literature and the original contributions of this work, Table A. 1 in Appendix A summarizes the origin and novelty status of

each key equation presented herein. The table is organized with columns for equation number, description, origin, novelty status, and notes.

6. Model Assumptions and Range of Validity

The analytical framework developed in this study is based on several theoretical foundations and simplifying assumptions. To ensure proper application and interpretation of the results, this section outlines the key assumptions, the range of validity of the predictions, and the conditions under which the model is expected to hold.

6.1. Summary of theoretical frameworks

The model integrates three main theoretical frameworks, as listed in Table 4.

Table 3. Requirements for applying the criterion to other models

Requirement	Description	Example of satisfaction
Existence of a dissipation function	The model must allow formulation of a dissipation potential as a function of strain rate and internal variables	Viscoplastic models with work-conjugate stress-strain rate pairs satisfy this
Differentiability	Θ must be differentiable with respect to strain rate to apply Eq. (12)	Most smooth viscoplastic models satisfy this; models with corners or discontinuities may require subdifferential calculus
Convexity	The dissipation function should be convex in strain rate to ensure a unique maximum and stable material response	Convexity is typical for stable dissipative materials and follows from the maximum dissipation principle itself
Incorporation of relevant physics	The model must capture the key mechanisms relevant to the phenomenon of interest	For semi-solid deformation, the model should include solid fraction dependence and rate sensitivity
Evolution equations for internal variables	The model must provide equations describing how internal variables evolve with deformation	Enables coupling between dissipation and microstructural evolution

Table 4. Summary of theoretical frameworks employed in the model

Theoretical framework	Primary references	Role in this study
Maximum rate of dissipation principle	Ziegler [22, 23]; Rajagopal & Srinivasa [24, 25]	Provides the thermodynamic foundation for stability analysis and the onset of localization (Eqs. (1-12))
Nguyen constitutive model for semi-solid deformation	Nguyen et al. [27]; Martin et al. [28]	Describes the viscoplastic flow behavior of semi-solid alloys at high solid fractions (Eqs. (13-15))
Granular mechanics/ critical state soil mechanics concepts	Gourlay et al. [13]; Kareh et al. [14]; Su et al. [15, 16]; Rudnicki & Rice [30]	Informs the interpretation of dilatancy, shear banding, and the granular-to-plastic transition

6.2. Key assumptions

The following assumptions, listed in Table 5, underlie the derivations and predictions presented in this work.

6.3. Range of validity

Based on the assumptions, the model's predictions are valid within the following ranges, as presented in Table 6.

Table 5. Summary of key assumptions and their justifications

Assumption	Description	Justification/ Limitation
Undrained conditions	Deformation occurs without liquid phase segregation; the liquid pressure equals the hydrostatic stress in the solid skeleton	Valid for strain rates $\geq 10^{-2}\ s^{-1}$ [26]. Below this threshold, liquid migration may occur, and the model should be extended to account for drainage effects
High solid fraction regime	The analysis focuses on solid fractions above the shear coherency point ($f_s > 0.4$), where a continuous solid skeleton exists, and granular mechanisms dominate	The Nguyen model [27] was calibrated for $f_s > 0.6$. The present results are most reliable in this range. Extrapolation to lower solid fractions should be approached with caution
Deviatoric stress state	Under undrained, high strain rate conditions, the total stress is predominantly deviatoric, with negligible mean stress contribution	Consistent with Suery & Flemings [26] and the assumptions of the Nguyen model [27]
Continuum representation	Microstructural features (grains, agglomerates, bonds) are represented implicitly through averaged material properties (e.g., ς, ψ, m)	Enables analytical tractability but does not capture local grain-scale heterogeneities. For systems with pronounced microstructural variability, discrete element methods [15, 16] may be more appropriate
Associated flow rule	The plastic strain rate is normal to the yield surface	Standard in classical plasticity; adopted in the Nguyen model [27] and consistent with the maximum dissipation framework
Isothermal conditions	Temperature is constant during deformation	Appropriate for high strain rate processes where adiabatic heating is negligible; validated by Nguyen et al. [27] for their experimental conditions
Cohesive granular behavior	Solid grains and agglomerates interact through cohesive bonds, which can break under shear, triggering dilatancy and localization	Supported by in-situ tomography studies [14-16] and consistent with critical state soil mechanics [30]
Yield surface shape (for internal friction interpretation)	The Hosford yield criterion [31] with exponent n describes the transition from granular to plastic behavior	The von Mises limit ($n = 2$, $\mu = 0.58$) provides an upper bound for internal friction; values for BCC ($n = 6$) and FCC ($n = 8$) metals are consistent with literature [32]

Table 6. Range of validity for key model parameters and conditions

Parameter/ Condition	Valid range	Notes/ Limitations
Solid fraction (f_s)	$f_s > 0.5$ (Qualitative trends valid above 0.4; quantitative predictions most reliable above 0.6)	Below 0.5, the solid skeleton may not be fully interconnected; granular mechanisms may differ [13]
Strain rate ($\dot{\varepsilon}$)	$\geq 10^{-2}$	Below this threshold, liquid segregation becomes significant, violating the undrained assumption [26]
Dilatancy (β)	$0 < \beta < 0.58$ (Typical range for granular materials)	Extreme values may require additional microstructural considerations
Localization parameter (α)	$\alpha \geq 5$ Marks onset of shear banding [17]	Derived from previous work; sensitivity analysis confirms robustness within ±20% variation
Temperature (T)	Isothermal conditions	Model does not account for temperature gradients or phase transformations
Microstructure	Granular, equiaxed grain morphology	The model may not capture effects of dendritic structures or highly elongated grains

7. Conclusions

In the present study, a new interpretation for the rheological features and deformation mechanisms of semi-solid materials has been proposed. For this purpose, an analytical criterion was developed by considering a constitutive model and applying the principle of the maximum rate of dissipation. The main findings of the analysis can be summarized as follows:

Rate-sensitivity plays a critical role in determining the active deformation mechanisms in the semi-solid state. It is demonstrated that there is a critical rate-sensitivity (m = 0.21), below that the deformation is associated with the rearrangement of the solid grains and agglomerates as well as the occurrence of the shear localization. On the other hand, at the rate-sensitivities above that critical value, the plastic deformation of grains is expected.

A correlation between the dilatancy value and the rate-sensitivity is established. The analysis reveals that within the granular deformation mode, the tendency for shear localization increases at higher solid fractions, which correspond to higher rate-sensitivity values. At critical state, where grains are interconnected via the cohesive bonds, the shear localization initiates by the local plastic deformation of grain bonds. This results in breaking the bonds between agglomerates and subsequent rearrangement of grains and Reynold's dilatancy.

Authors' contributions

M. H. Sheikh Ansari: Conceptualization, Investigation, Writing original draft preparation

M. Aghaie Khafri: Conceptualization, Reviewing & editing, Supervision

Conflict of interest

The authors declare that they have no conflict of interest.

Funding

This research did not receive any specific grant from funding agencies in the public, commercial, or not-for-profit sectors.

Data availability

Data available on request from the authors.

8. References

[1] Atkinson, H. V. (2005). Modelling the semi-solid processing of metallic alloys. *Progress in Materials Science*, *50*(3), 341-412. https://doi.org/10.1016/j.pmatsci.2004.04.003

[2] Wang, W., Guo, E., Phillion, A. B., Eskin, D. G., Wang, T., & Lee, P. D. (2020). Semi-solid compression of nano/micro-particle reinforced Al-Cu composites: An in-situ synchrotron tomographic study. *Materialia*, *12*, 100817. https://doi.org/10.1016/j.mtla.2020.100817

[3] Li, H., Cao, M., Niu, L., Huang, K., & Zhang, Q. (2021). Establishment of macro-micro constitutive model and deformation mechanism of semi-solid Al6061. *Journal of Alloys and Compounds*, *854*, 157124. https://doi.org/10.1016/j.jallcom.2020.157124

[4] Wang, K., Wang, L., Li, F., Zhang, Z., & Luo, R. (2022). Anisotropic microstructure and thixo-compression deformation behavior of extruded 7075 aluminum alloy in semi-solid state. *Materials Science and Engineering: A*, *833*, 142514. https://doi.org/10.1016/j.msea.2021.142514

[5] Liu, Z., Zhou, R., Xiong, W., He, Z., Liu, T., & Li, Y. (2022). Compressive rheological behavior and microstructure evolution of a semi-solid CuSn10P1 alloy at medium temperature and low strain. *Metals 2022*, *12*(1), 143. https://doi.org/10.3390/met12010143

[6] Boluri Gashti, A. H., Abedi, H. R., & Salehi, M. T. (2023). Microstructure evolution and constitutive modeling of as-cast A356 aluminum alloy in semi-solid deformation regime. *Journal of Materials Research and Technology*, *24*(18), 7720-7731. https://doi.org/10.1016/j.jmrt.2023.05.025

[7] Burgos, G. R., Alexandrou, A. N., & Entov, V. (2001). Thixotropic rheology of semi-solid metal suspensions. *Journal of Materials Processing Technology*, *110*(2), 164-176. https://doi.org/10.1016/S0924-0136(00)00731-7

[8] Modigell, M., & Koke, J. (2001). Rheological modelling on semi-solid metal alloys and simulation of thixocasting processes. *Journal of Materials Processing Technology*, *111*(1-3), 53-58. https://doi.org/10.1016/S0924-0136(01)00496-4

[9] Cézard, P., Favier, V., Bigot, R., Balan, T., & Berveiller, M. (2005). Simulation of semi-solid thixoforging using a micro-macro constitutive equation. *Computational Materials Science*, *32*(3-4), 323-328. https://doi.org/10.1016/j.commatsci.2004.09.036

[10] Favier, V., & Atkinson, H. V. (2011). Micromechanical modelling of the elastic-viscoplastic response of metallic alloys under rapid compression in the semi-solid state. *Acta Materialia*, *59*(3), 1271-1280. https://doi.org/10.1016/j.actamat.2010.10.059

[11] Wang, J., Phillion, A. B., & Lu, G. (2014). Development of a viscoplastic constitutive modeling for thixoforming of AA6061 in semi-solid state. *Journal of Alloys and Compounds*, *609*, 290-295. https://doi.org/10.1016/j.jallcom.2014.04.140

[12] Koeune, R., & Ponthot, J. P. (2014). A one phase thermomechanical model for the numerical simulation of semi-solid material behavior. Application to thixoforming. *International Journal of Plasticity*, *58*, 120-153. https://doi.org/10.1016/j.ijplas.2014.01.004

[13] Gourlay, C. M., Dahle, A. K., Nagira, T., Nakatsuka, N., Nogita, K., Uesugi, K., & Yasuda, H. (2011). Granular deformation mechanisms in semi-solid alloys. *Acta Materialia*, *59*(12), 4933-4943. https://doi.org/10.1016/j.actamat.2011.04.038

[14] Kareh, K. M., Lee, P. D., Atwood, R. C., Connolley, T., & Gourlay, C. M. (2014). Revealing the micromechanisms behind semi-solid metal deformation with time-resolved X-ray tomography. *Nature Communications 2014 5:1*, *5*(1), 4464. https://doi.org/10.1038/ncomms5464

[15] Su, T. C., O'Sullivan, C., Yasuda, H., & Gourlay, C. M. (2020). Rheological transitions in semi-solid alloys: In-situ imaging and LBM-DEM simulations. *Acta Materialia*, *191*, 24-42. https://doi.org/10.1016/j.actamat.2020.03.011

[16] Su, T. C., O'Sullivan, C., Nagira, T., Yasuda, H., & Gourlay, C. M. (2019). Semi-solid deformation of Al-Cu alloys: A quantitative comparison between real-time imaging and coupled LBM-DEM simulations. *Acta Materialia*, *163*(7123), 208-225. https://doi.org/10.1016/j.actamat.2018.10.006

[17] Ansari, M. H. S., & Aghaie Khafri, M. (2017). Predicting flow localization in semi-solid deformation. *International Journal of Material Forming 2017 11:2*, *11*(2), 165-173. https://doi.org/10.1007/s12289-017-1339-6

[18] Sheikh Ansari, M. H., & Aghaie Khafri, M. (2018). Shear localization in semi-solid deformation: A bifurcation theory approach. *Mechanics Research Communications*, *89*, 1-5. https://doi.org/10.1016/j.mechrescom.2018.02.002

[19] Sheikh Ansari, M. H., & Aghaie Khafri, M. (2018). An extension of Rice localization criterion to predict the onset of shear localization in semi-solid materials. *International Journal of Material Forming 2018 12:4*, *12*(4), 703-716. https://doi.org/10.1007/s12289-018-1445-0

[20] Sheikh Ansari, M. H., & Aghaie Khafri, M. (2019). Constitutive modeling of semi-solid deformation for the assessment of dilatant shear bands. *Applied Mathematical Modelling*, *70*, 128-138.

https://doi.org/10.1016/j.apm.2019.01.028

[21] Esquivel, E. V., & Murr, L. E. (2005). Grain boundary contributions to deformation and solid-state flow in severe plastic deformation. *Materials Science and Engineering: A*, *409*(1-2), 13-23. https://doi.org/10.1016/j.msea.2005.04.063

[22] Ziegler, H. (1963). *Progress in solid mechanic*, (Sneddon, I. N., Hill, R., Ed.), New York, 93-193

[23] Ziegler, H. (1983). *An introduction to thermomechanics* (1st Ed.). North-Holland Publishing Company

[24] Rajagopal, K. R., & Srinivasa, A. R. (1998). Mechanics of the inelastic behavior of materials-part 1, theoretical underpinnings. *International Journal of Plasticity*, *14*(10-11), 945-967. https://doi.org/10.1016/S0749-6419(98)00037-0

[25] Rajagopal, K. R., & Srinivasa, A. R. (1998). Mechanics of the inelastic behavior of materials. Part II: Inelastic response. *International Journal of Plasticity*, *14*(10-11), 969-995. https://doi.org/10.1016/S0749-6419(98)00041-2

[26] Suery, M., & Flemings, M. C. (1982). Effect of strain rate on deformation behavior of semi-solid dendritic alloys. *Metallurgical Transactions A 1982*, *13*(10), 1809-1819. https://doi.org/10.1007/bf02647837

[27] Tzimas, E., & Zavaliangos, A. (1999). Mechanical behavior of alloys with equiaxed microstructure in the semi-solid state at high solid content. *Acta Materialia*, *47*(2), 517-528. https://doi.org/10.1016/S1359-6454(98)00356-5

[28] Nguyen, T. G., Favier, D., & Suery, M. (1994). Theoretical and experimental study of the isothermal mechanical behavior of alloys in the semi-solid state. *International Journal of Plasticity*, *10*(6), 663-693. https://doi.org/10.1016/0749-6419(94)90028-0

[29] Martin, C. L., Brown, S. B., Favier, D., & Suéry, M. (1995). Shear deformation of high solid fraction (> 0.60) semi-solid Sn-Pb under various structures. *Materials Science and Engineering: A*, *202*(1-2), 112-122. https://doi.org/10.1016/0921-5093(95)09797-X

[30] Rudnicki, J. W., & Rice, J. R. (1975). Conditions for the localization of deformation in pressure-sensitive dilatant materials. *Journal of the Mechanics and Physics of Solids*, *23*(6), 371-394. https://doi.org/10.1016/0022-5096(75)90001-0

[31] Hosford, W. F. (1972). A generalized isotropic yield criterion. *Journal of Applied Mechanics*, *39*(2), 607-609. https://doi.org/10.1115/1.3422732

[32] Butcher, C., & Abedini, A. (2017). Shear confusion: Identification of the appropriate equivalent strain in simple shear using the logarithmic strain measure. *International Journal of Mechanical Sciences*, *134*, 273-283. https://doi.org/10.1016/j.ijmecsci.2017.10.005

[33] Ferrante, M., & De Freitas, E. R. (2001). Rheological behavior and deformation characteristics of a commercial and a laboratory-cast Al-4% Cu alloy in the semi-solid state. *Acta Materialia*, *49*(18), 3839-3847. https://doi.org/10.1016/S1359-6454(01)00239-7

[34] Narumi, T., Ohta, K., Ohta, M., Numata, T., Asahi, K., Katsube, R., & Yasuda, H. (2023). Observation of grain motion during semi-solid deformation by using 4D-CT and 3D-XRD. *IOP Conference Series: Materials Science and Engineering*, *1274*(1), 012053. https://doi.org/10.1088/1757-899x/1274/1/012053

[35] Su, T. C., O'sullivan, C., Yasuda, H., & Gourlay, C. M. (2022). Understanding the rheological transitions in semi-solid alloys by a combined in-situ imaging and granular micromechanics modeling approach. *Solid State Phenomena*, *327*, 127-132. https://doi.org/10.4028/www.scientific.net/SSP.327.127

[36] Wu, M., Liu, Y., Wang, T., & Yu, K. (2016). Deformation behavior and characteristics of sintered porous 2024 aluminum alloy compressed in a semi-solid state. *Materials Science and Engineering: A*, *674*, 144-150. https://doi.org/10.1016/j.msea.2016.07.120

[37] Zhang, C., Zhao, S., Yan, G., & Wang, Y. (2018). Deformation behavior and microstructures of semi-solid A356.2 alloy prepared by radial forging process during high solid fraction compression. *Proceedings of the Institution of Mechanical Engineers, Part B: Journal of Engineering Manufacture*, *232*(3), 487-498. https://doi.org/10.1177/0954405416646002

[38] Chino, Y., Kobata, M., Iwasaki, H., & Mabuchi, M. (2003). An investigation of compressive deformation behavior for AZ91 Mg alloy containing a small volume of liquid. *Acta Materialia*, *51*(11), 3309-3318. https://doi.org/10.1016/S1359-6454(03)00162-9

[39] Chen, Y., Yuan, Z., Zhan, H., Zhao, Y., Song, X., Wang, G., & Gu, Y. (2017). Unexpected dynamic recrystallization behavior of Ti-7Cu alloy in semi-solid state. *Journal of Alloys and Compounds*, *712*, 468-476. https://doi.org/10.1016/j.jallcom.2017.04.091

[40] Sheikh Ansari, M. H., & Aghaie Khafri, M. (2019). Effect of semi-solid deformation on the restoration mechanisms and texture evolution in AA7075. *JOM 2019*, *71*(12), 4696-4704. https://doi.org/10.1007/s11837-019-03835-8

[41] Jiang, J., Liu, Y., Xiao, G., Wang, Y., & Xiao, X. (2020). Effects of plastic deformation of solid phase on mechanical properties and microstructure of wrought 5A06 aluminum alloy in directly semi-solid thixoforging. *Journal of Alloys and Compounds*, *831*, 154748. https://doi.org/10.1016/j.jallcom.2020.154748

[42] Prasad, Y. V. R. K., & Rao, K. P. (2011). Materials modeling and finite element simulation of isothermal forging of electrolytic copper. *Materials & Design*, *32*(4), 1851-1858. https://doi.org/10.1016/j.matdes.2010.12.018

[43] Gupta, A. K., Krishnamurthy, H. N., Singh, Y., Prasad, K. M., & Singh, S. K. (2013). Development of constitutive models for dynamic strain aging regime in austenitic stainless steel 304. *Materials & Design*, *45*, 616-627. https://doi.org/10.1016/j.matdes.2012.09.041

[44] Alaneme, K. K., Kareem, S. A., & Bodunrin, M. O. (2023). Hyperbolic-sine constitutive model determined hot deformation mechanisms and workability response of Al-Zn/ Cu and Al-Zn/ SiC based composites. *Results in Engineering*, *19*, 101255. https://doi.org/10.1016/J.RINENG.2023.101255

[45] Xu, X., Zhang, P., Fang, J., Wen, L., Yang, Y., Zhao, Y., & Chen, L. (2024). The hot deformation behavior and processing map analysis of a high-nitrogen austenitic stainless steel. *Journal of Materials Research and Technology*, *33*, 1359-1365. https://doi.org/10.1016/j.jmrt.2024.09.162

[46] Li, X., Hao, Y., Wang, Y., Shi, H., Wang, X., Hu, X., & Yu, J. (2024). Hot deformation and processing map of in-situ graphene reinforced magnesium matrix nanocomposites. *Journal of Alloys and Compounds*, *1005*, 175978. https://doi.org/10.1016/j.jallcom.2024.175978

[47] Xiao, Y., Deng, Y., An, Y., Yuan, L., Zhan, X., & Wang, B. (2024). Strain rate affects the deformation mechanism of a Ti-55511 titanium alloy: Modeling of constitutive model and 3D processing map using machine learning. *Materials Today Communications*, *40*, 109881. https://doi.org/10.1016/j.mtcomm.2024.109881

APPENDIX A: Classification of Equation Origins

This appendix provides a comprehensive classification of all key equations presented in the main text, distinguishing between established results from the literature and original contributions of this work. The classification aims to ensure transparency and proper attribution, while clearly highlighting the novel developments introduced in this study.

Table A. 1. Classification of equations: established vs. novel contributions

Equation	Description	Novelty status	Notes
Eq. (1)	Rate of dissipation	Established	Fundamental thermodynamic relation
Eq. (2)	Helmholtz free energy dependence	Established	Standard form in finite deformation plasticity
Eq. (3)	Plastic velocity gradient	Established	Standard kinematic relation
Eqs. (4-6)	Derivation of dissipation rate in terms of L_p	Established	Follows from the maximum dissipation framework
Eqs. (7, 8)	Maximum dissipation principle inequality	Established	Core thermodynamic principle
Eqs. (9-11)	Stability condition derivation	Established framework, new application	Applied specifically to semi-solid deformation
Eq. (12)	Onset of localization	Novel	First application of maximum dissipation principle to shear localization in semi-solid materials
Eq. (13)	Constitutive model for semi-solid deformation	Established	Original model from literature
Eq. (14)	Solid fraction function	Established	Empirical constant from experiments
Eq. (15)	Stress as function of strain rate	Rearranged form	Algebraic manipulation for dissipation calculation
Eq. (16)	Dissipation function	Novel	First explicit dissipation function for semi-solid deformation combining Nguyen model with maximum dissipation framework
Eqs. (17, 18)	Localization condition applied to dissipation function	Novel	First application of Eq. (12) to semi-solid constitutive model
Eq. (19)	Localization criterion	Novel	New criterion linking rate-sensitivity, solid fraction, and localization
Eq. (20)	Reformulated with total porosity fraction	Novel	Extension to include porosity evolution
Eq. (21)	Porosity evolution	New combination	First application of Gurson-type evolution to semi-solid deformation with solid skeleton fraction ψ
Eq. (22)	Initial solid skeleton fraction	Novel	New parameter linking solid fraction to skeleton connectivity

Table A. 1. *Continued*

Equation	Description	Novelty status	Notes
Eq. (23)	Total derivative of f with respect to $\dot{\gamma}$	Novel	Required for localization analysis
Eqs. (24, 25)	Reformulated localization condition	Novel	Intermediate steps in the derivation
Eq. (26)	Introduction of localization parameter	Novel	New parameter quantifying strain localization intensity
Eq. (27)	Critical localization condition	Novel	New criterion; numerical value $\alpha_c = 5\alpha_c = 5$ from previous work [17]
Eq. (28)	Dilatancy as function of rate-sensitivity	Novel	Central result of the paper
Eq. (29)	Numerical form of β	Novel	New quantitative relationship with numerical values
Eq. (30)	Hosford yield criterion	Established	Used for interpreting internal friction limits